Applied Physics Letters

A broadband acoustic panel based on double-layer membrane-type metamaterials

Cite as: Appl. Phys. Lett. **118**, 184101 (2021); https://doi.org/10.1063/5.0042584
Submitted: 31 December 2020 . Accepted: 16 April 2021 . Published Online: 03 May 2021

Huy Nguyen, Qian Wu, Jiaji Chen, Yukai Yu, Hui Chen, Sharon Tracy, and Guoliang Huang

Applied Physics Letters ARTICLE scitation.org/journal/apl

A broadband acoustic panel based on double-layer membrane-type metamaterials

Cite as: Appl. Phys. Lett. **118**, 184101 (2021); doi: 10.1063/5.0042584
Submitted: 31 December 2020 · Accepted: 16 April 2021 ·
Published Online: 3 May 2021

Huy Nguyen,[1] Qian Wu,[1] Jiaji Chen,[1] Yukai Yu,[1] Hui Chen,[1] Sharon Tracy,[2] and Guoliang Huang[1,a)]

AFFILIATIONS

[1]Department of Mechanical and Aerospace Engineering, University of Missouri, Columbia, Missouri 65211, USA
[2]Materials Innovation, Steelcase Inc., Grand Rapids, Michigan 49508, USA

Note: This Paper is part of the APL Special Collection on Metastructures: From Physics to Applications.
[a)]**Author to whom correspondence should be addressed:** huangg@missouri.edu

ABSTRACT

Low-frequency noise is a growing problem in large structures of modern transportation technologies. In this study, we report a large-scale acoustic panel made of double-layer membrane-type metamaterials (DMAMs) for broadband noise reduction. A complete theoretical model based on the unit cell is fully developed and extended for finite multi-celled membrane-type acoustic metamaterial (MAMs) array. A large-scale acoustic panel constructed from 8×8 DMAM unit cells is proposed. To deal with the global compliance of the large-scale support structure, the double-layer panel frame structure with large bending stiffness is designed to shift the global resonances to higher frequencies and provide an efficient way to well maintain the MAM's performance. Moreover, the double-layer configuration further guarantees ultra high transmission loss within the frequency range of interest. Experiments are carried out to validate the analytical and numerical predictions. Excellent transmission loss ranging from 20 to 59 dB within ten third octave bands (0.32–2.5 kHz) is observed, deeply breaking the mass density law. We believe the proposed design and the associated theoretical model could serve as an efficient tool for designing acoustic metamaterial-based panels and soundproof walls with high noise reduction in low/middle frequency regions.

Low-frequency sound reduction always challenges scientists due to the limited acoustic performance of traditional materials, whose design and performance are limited by laws of nature, such as mass density, quarter wavelength laws, and so forth.[1–6] Most of the traditional sound proofing walls therefore are either cumbersome or sturdy to exploit the stiffness control region.[7–9] New approaches to control the low-frequency sound propagation in the form of new materials are extremely desirable.

Recently, acoustic metamaterials have been gaining attention, showing counter-intuitive properties that are not found in nature, such as negative mass density, negative bulk modulus, double negative materials, and so forth.[9–15] Realization of a lightweight acoustic panel possessing high transmission loss (TL) at low frequencies is one of the most promising potential applications of the acoustic metamaterials. Yang *et al.*[12] have suggested that a membrane-type acoustic metamaterial (MAM) based on a thin and soft membrane with an attached mass in the center supports negative effective mass density within the frequency region slightly before the antiresonant frequency. At the antiresonance where the MAM's average normal displacement vanishes, the transmitted sound is dramatically suppressed, consequently making the MAM an acoustically hard wall.[16–18] The working region therefore can be tuned by adjusting the resonant frequencies of the MAM.[16,19,20] However, most of the existing results are so far limited in the unit cell scale and quite difficult to be transferred to large-scale products since the fixed rim or periodic boundary conditions employed in unit cell studies can hardly be practiced in large-scale products. The support frame for a large-scale panel inevitably suppresses the low-frequency sound reduction performance due to the emergence of additional global resonances from the frame. Aside from the MAM, plate-type acoustic metamaterials have also been proposed for noise reduction applications. Although a plate-type acoustic metamaterial unit cell exhibits great sound reduction performance,[19] its performance drops significantly in the large-scale panel configuration.[21] The synergetic coupling in a plate-type acoustic metamaterial supercell, supporting four weakly coupled resonances (TL peaks), was proposed for low-frequency sound reduction.[22] However, its improvement over the mass density law is still limited and only demonstrated within narrow bands. Other plate-type acoustic metamaterial designs by embedding coupled cavities within a unit cell[23] realized TL enhancement based on coupling modes. The performance of this

design is mainly affected by the stiffness control region; the observed benefit given by the coupling only takes place within a narrow band. Therefore, in order to achieve optimal sound reduction performance in a large-scale metamaterial panel, optimized unit cell performance and suppression of the panel vibration are essential.

In this research, we present an acoustic panel made of a multi-celled double-layer membrane-type acoustic metamaterial (DMAM) array to achieve ultra large sound transmission loss. The proposed panel is fully characterized by the theoretical models of the MAM and DMAM, which are numerically validated. The supporting frame of the proposed panel is designed to be lightweight and possess high bending stiffness in order to increase the frequency of its vibration and thus suppress the adverse effect on the overall sound reduction performance within low-frequency regions. The frame vibration is also investigated to optimize the working region of the panel. By choosing proper design parameters, excellent transmission loss performance can be obtained in the panel configuration at low frequencies, which are also evidenced by experimental testings.

The design of our proposed acoustic panel is illustrated in Fig. 1(a). It is composed of 8 × 8 DMAM unit cells supported by an elastic frame. All geometrical and material properties of the panel are listed in Table I. Each unit cell comprises two MAM components, connected through an elastic frame, as indicated in Fig. 1(b). As will be discussed later, we employ the I-beam design for the support frame since it generates large bending stiffness and therefore exhibits resonance effect at higher frequencies [see Fig. 1(c)]. Note that the global resonances mainly depend on the height of the I beam (h). The thickness t_w barely affects the resonances due to the fact that the bending stiffness is a cubic function of t_w. We start with the theoretical investigation on the DMAM unit cell. Since the supporting frame panel has non-trivial thickness ($h = 63$ mm), resulting in large bending stiffness,[24] the DMAM unit cells can be considered to have nearly fixed boundary

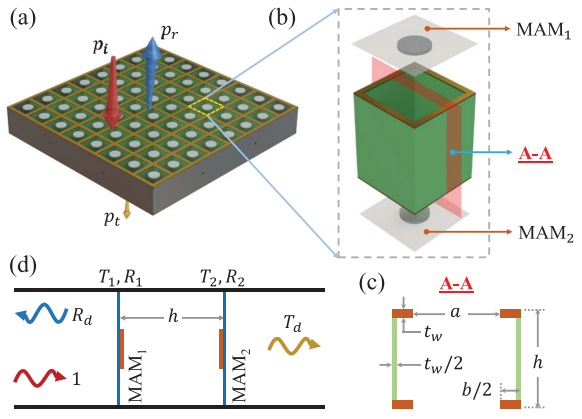

FIG. 1. (a) Schematic of the proposed large-scale acoustic panel design. The incident sound (p_i) wave is mostly reflected (p_r), resulting in strongly suppressed sound transmission (p_t). (b) Detailed view of the double-layer membrane-type acoustic metamaterial unit cell. It is assembled from two membrane-type acoustic metamaterial unit cells and the gridded-like elastic frames. (c) Sectional view of the frame. All the geometric parameters are indicated. The parts of different colors are all made of aluminum. (d) Schematic of the acoustic model of a double-layer membrane-type acoustic metamaterial unit cell in the tube environment. An incident sound wave of normalized amplitude is considered. T_d and R_d denote the transmitted and reflected waves, respectively.

TABLE I. The acoustic panel's parameters.

Element	Properties	Value
Unit cell size	Width × height	50 mm × 50 mm
	Thickness: h	63 mm
Membrane	Young's modulus	1.08 GPa
	Mass density	960 kg/m^3
	Poisson's ratio	0.48
	Thickness	0.076 mm
	Loss factor	796 Pa·s
	Pre-tension	5 MPa
Mass	Material	Aluminum
	Diameter	21.59 mm
	Thickness	2 mm
Panel frame	Material	Aluminum
	Web and flange thickness: t_w	1 mm
	Grid-cut size: a × a	42 mm × 42 mm

conditions on the lateral sides in the unit cell analysis. When a noise source is located far from the panel, the incoming noise sound can be treated as normal incidence. As theoretically sketched in Fig. 1(d), under the normalized incidence ($p_i = e^{-ikx}$), the transmission and reflection coefficients are defined as[25]

$$T_d = \frac{\vartheta T_1 T_2}{1 - R_1 R_2 \vartheta^2} \quad \text{and} \quad R_d = R_1 + \frac{T_1^2 R_2 \vartheta^2}{1 - R_1 R_2 \vartheta^2}, \tag{1}$$

respectively, where $\vartheta = e^{-ikh}$, (T_1, R_1), and (T_2, R_2) are the phase shift factor between two MAMs, transmission and reflection coefficients of the MAM$_1$ and MAM$_2$, respectively. These coefficients can be obtained from theoretical,[16,17] simulation,[13] or experimental[26] results for a single MAM unit cell. In this research, to keep the design and fabrication simple, two identical MAM components are chosen, i.e., $T = T_1 = T_2$ and $R = R_1 = R_2 = 1 - T$.[17] Then, the TL of the MAM (TL$_s$) and DMAM (TL$_d$) unit cells can be defined as

$$\begin{aligned} \mathrm{TL}_s &= -20 \times \log_{10}|T|, \\ \mathrm{TL}_d &= 2 \times \mathrm{TL}_s + 20 \times \log_{10}|1 - (\vartheta R)^2|, \end{aligned} \tag{2}$$

respectively, which reveals that in the vicinity of the antiresonances ($R \to 1$), TL$_d$ is at least twice as high as TL$_s$.[25] Therefore, in order to achieve optimized sound reduction performance in the DMAM unit cell, the TL of the MAM component must be optimized. In addition, TL$_d$ reaches dips and peaks at the MAM resonances ($T \to 1$) and antiresonances ($|T| \to 0$),[12,27] respectively. In other words, the location of MAM TL dips and peaks will be preserved in the DMAM unit cell. The antiresonance at low frequencies is a result of the hybridization between the first resonance mode (named mass mode where the mass oscillates strongly) and the second resonance mode (named membrane mode where the mass is stationary but the membrane vibrates) (see the supplementary material). Therefore, it is also called hybrid mode[26] and locates closer to the first resonance mode than the second one does since the former is stronger in intensity. The working region defined as the region centered at the anti-resonance and

covering high TL spectrum can be tuned by adjusting the first two resonances of the MAM component. In other words, the working region mainly depends on the spectral distance between two modes.

In the MAM, since the membrane is very lightweight and hardened by pre-tension,[12,13] the second resonance mode's frequency can be tuned far away from the first resonance mode,[16,28] mainly affected by the attached mass. In this way, a broad working region is expected for the MAMs with large pre-tension. Figure 2(a) shows the TL of the MAM component under different membrane pre-tension conditions. It can be confirmed that when the pre-tension is increased, the first resonance mode is slightly shifted to higher frequencies, while the second resonance mode shifts in a more significant way. In other words, increasing the pre-tension leads to a greater spectral distance between two modes and hence a larger working region. Therefore, adjusting pre-tension is an efficient way to control the working region of the MAM components while the weight and shape remaining unchanged. Considerably large pre-tension may challenge the fabrication and longevity due to the creeping of the MAM over the time. In this research, 5 MPa pre-tension on the membrane is selected in the DMAM unit cell. With such a MAM configuration [red curve in Fig. 2(a)], one dip and one peak appear corresponding to the first MAM resonance and antiresonance located at 211 and 545 Hz, respectively.

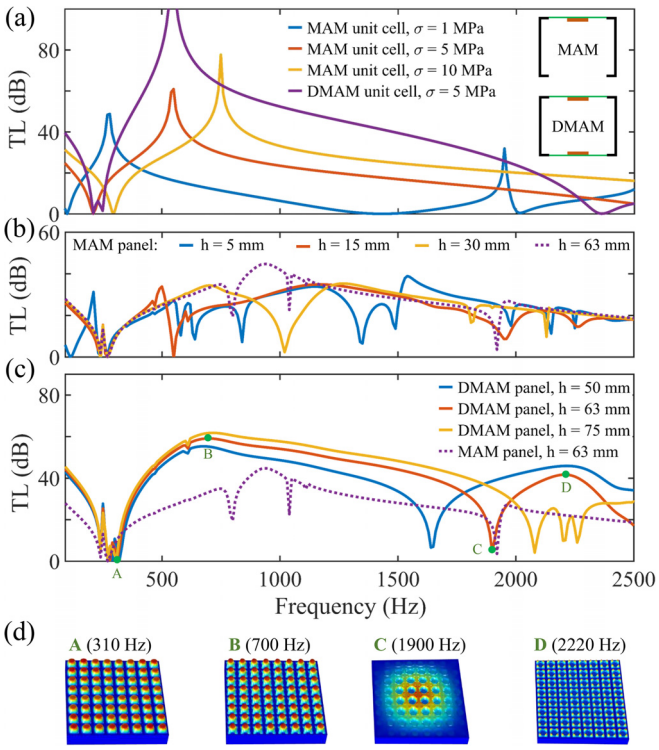

FIG. 2. (a) Transmission loss spectra of the single MAM unit cell under different membrane pre-tension conditions (σ) and the DMAM unit cell comprised from two identical MAMs under a pre-tension of 5 MPa. Comparison of TL spectra of (b) MAM panels and (c) DMAM panels with different thicknesses of the panel thickness when a pre-tension of 5 MPa is employed on the membranes. (d) The mode shapes of the DMAM panel of the highlighted peaks and dips.

The DMAM unit cell constructed by two selected MAMs separated by 63 mm is studied and the corresponding result is presented by the purple curve in Fig. 2(a) purposely to compare its performance with the single MAM component. Obviously, the TL of DMAM unit cell TL_d is significantly higher than that of the single MAM component (red curve) TL_s. Within most regions except for the vicinity of the MAM resonance, TL_d is nearly twice as high as TL_s and the peak and dip of the MAM are preserved in the DMAM configuration. These observations confirm the advantage of DMAM unit cell over the single MAM component discussed previously. Other than the TL dips inherited from the MAM component, additional dips [250, 2360, and 3350 Hz (see the supplementary material)] emerge in the DMAM configuration. In fact, they are a consequence of Fabry–Pérot resonances between the two MAM components.[15,25] In summary, there still exists a continuous broadband TL spectrum of at least 25 dB covering the range from 0.28 to 2 kHz.

Generally, acoustic panels, constructed by attaching unit cells on a grid-like elastic frame, have low bending stiffness if the unit cell is thin, for instance, a MAM unit cell held on a thin frame.[19,20,22] In real applications, the panel edges are often constrained, leading to several panel vibration modes distributed at low frequencies. These vibration modes cause strong but unavoidable interference of these modes on the local modes of unit cells. Consequently, the design performance of the unit cell is heavily undermined.[19,23] Therefore, in addition to the need of excellent performance of unit cell, a high bending stiffness of the panel frame is another requirement for optimized sound reduction performance. Figure 2(b) illustrates the TL spectra of the MAM panels ($\sigma = 5$ MPa) with different panel thicknesses. Clearly, when the thickness is small, multiple TL dips, which do not exist in the unit cell analysis, appear within the low-frequency region. With the increased thickness, the dips exhibit blueshifts as the panel vibration resonances go to higher frequencies due to the higher bending stiffness the panel possesses. Especially, when the thickness is 63 mm, the performance of the unit cell within the frequency region of interest is nearly conserved in the panel configuration with the dampening and blueshift of the TL peak.

Similarly, a DMAM panel with an appropriate thickness is expected to perform better than the corresponding MAM panel by well preserving the performance of the DMAM unit cell. To examine and optimize the performance of the DMAM panel, we conduct parametric study on the thickness of the panel frame. As shown in Fig. 2(c), the TL of the DMAM panel is much higher than that of the single MAM. The TL of the DMAM unit cell [purple curve in Fig. 2(a)] remains in the panel configuration, especially on the left side of the TL peak (point B). In contrast, the TL after point B is lowered when decreasing the panel frame thickness. For the chosen thickness of 63 mm, the TL dip (point C) is induced by the first-order panel vibration resonance, as can be realized through the mode shape presented in Fig. 2(d) where the frame oscillates strongly. Interestingly, an extra TL peak (point D) emerges thanks to the panel vibration resonance, bringing satisfactory sound reduction performance within the region where the TL is trivial in the unit cell analysis [purple curve in Fig. 2(a)]. Points A and D show the first and second resonance modes of the MAM, respectively [see Fig. 2(d)]. While the former manifests as a dip as in the DMAM configuration, the latter weakly couples with the vibration of the frame to form a peak (see the supplementary material). Figure 2(d) also shows that the mode shape at point B resembles

the anti-resonance of the MAM of which the locally optimal performance is undermined and gets shifted to the higher frequency (545–700 Hz) due to the interference with the vibration of the panel. Due to the large bending stiffness, the panel frame vibrates in a much smaller amplitude than the mass and membrane do at points B and D. Therefore, the local mode shapes are dominant in the coupling mode shapes to produce TL peaks, as observed in Fig. 2(d) and the supplementary material. It is noteworthy that due to the effect of the global mode, the first resonance mode shifts from 211 to 310 Hz. In short, despite the presence of the mode shifting and the global mode, a broadband TL region at 25–59 dB is still noticeable from 0.35 to 2.85 and 1.85 to 2.4 kHz in the panel.

To illustrate the practical application, we fabricate an acoustic panel sample following the parameters provided in Table I [Fig. 3(a)]. The panel frame is an assembly of web bars and flange plates (see the supplementary material), which are designed deliberately and fabricated by a CNC machine. They are then bonded together by super glue. The membranes are cut from a polyethylene clear sheet, and the pre-tension is applied using a stretching machine; see Fig. 3(a). This ensures that the pre-tension strengths in all unit cells are uniform and thus suppress couplings between neighboring units. The circular masses are speedily produced on a punching machine and attached to the membranes with super glue. The finalized DMAM panel is shown in Fig. 3(b). To experimentally test the sound insulation performance of the sample, small semi-anechoic chamber as described in Fig. 3(c) is fabricated. The plane wave-like noise sound is generated from a 16 in. loudspeaker placed far away from the sample at the inlet of the chamber. An acoustic foam of thickness 8 in., backed by a 2 in.-thick air cavity, is then installed on the end of the receiving chamber. Some thinner foam layers are then attached on the inner side walls to make the outlet an anechoic chamber. All the employed foams can efficiently absorb the sound waves even within the low-frequency range (see the supplementary material). A commercial software Bruel Kjaer PULSE Labshop is then utilized to conduct the measurement. We use Labshop, through the LAN XI, to generate a noise signal ranging from 0.08 to 3.2 kHz. The signal is later amplified by a power amplifier before being sent to a high-power loudspeaker. A 1/2 in. Bruel Kjaer free-field condenser microphone (type 4966-H-041) with a high-temperature pre-amplifier (type 1706) is used to measure the pressure amplitudes inside the anechoic chamber on a matrix of 5×5 points on a plane 4 in. distance from the sample. The measurement is proceeded in two steps.[29] First, the background pressure amplitude is measured in the absence of the sample. Later, the transmitted pressure amplitude is measured after the sample is installed. The noise reduction is then calculated from the pressure measured. Besides the experimental result, the simulation result and mass density law are also presented for comparison, as shown in Fig. 3(d). The experimental result shows excellent agreement with the simulation result and deeply breaks the mass density law in the region 0.37–1.5 kHz. TL exceeding 20 dB at almost all frequencies within the range 0.32–2.5 kHz and that ranging 40–59 dB from 0.45 to 1.48 kHz were recorded. More importantly, the proposed DMAM panel with frame vibration suppressed outperforms the acoustic panel previously reported in which the efficient sound insulation range only covers 50–1000 Hz.[30] Moreover, the acoustic panel is optically transparent as well by using transparent plastic sheets as the membranes.

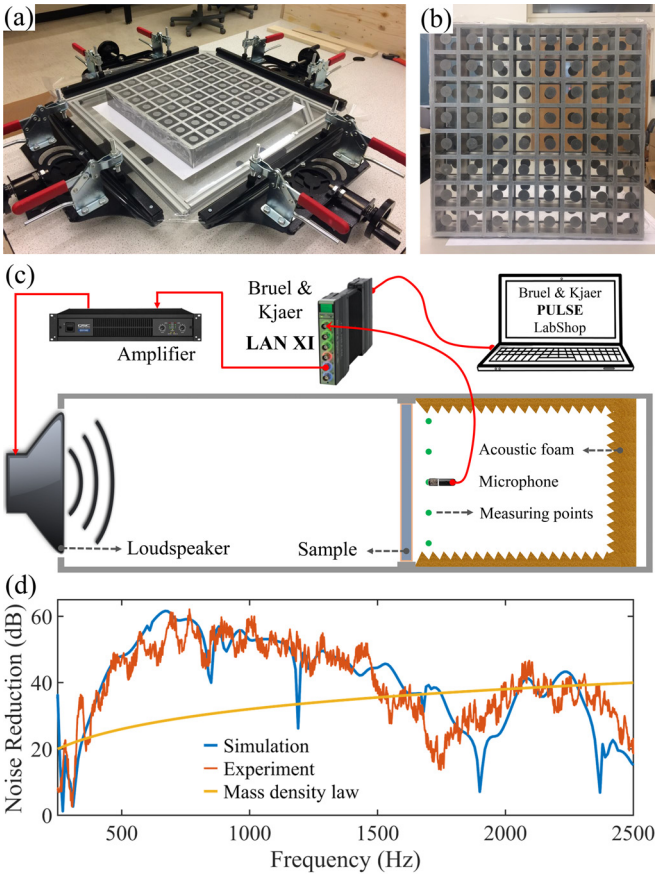

FIG. 3. (a) Photograph of stretching the membrane in the acoustic panel. The pre-tension on the membrane can be easily adjusted. (b) Photograph of the large-scale double-layer membrane-type acoustic metamaterial-based panel. (c) Schematic illustration of the experimental setup. The foam layer within the tube cross section is of a thickness of 8 in. A 2 in.-thick air cavity is arranged next to the foam. (d) Comparison between the simulation and experimental results for the sample shown in (b). The noise reduction performance according to the conventional mass density law is also presented for illustrating how well the large-scale double-layer membrane-type acoustic metamaterial-based panel performs.

In summary, the double-layer membrane-type acoustic metamaterial has been proposed and studied thoroughly by both theoretical and numerical analyses, which indicates that the transmission loss of the proposed DMAM unit cell is at least twice as high as that of the MAM configuration around the anti-resonance. An acoustic panel based on an 8×8 DMAM array is then proposed to achieve broadband noise reduction. The experimental result shows excellent transmission loss spectrum overall exceeding 20 dB within the range 0.32–2.5 kHz. Specifically, transmission loss ranging 40–59 dB within 0.45–1.48 kHz deeply breaks the mass density law. In addition, the proposed panel is almost optically transparent, which is essential from an esthetic standpoint. We believe that the proposed design and the associated theoretical model may pave the way for designing highly efficient and lightweight acoustic panels and barriers with broadband operations at low/middle frequencies.

See the supplementary material for the complete illustration of Fig. 2, some experimental details, and the exploded view of the experimental panel sample.

AUTHORS' CONTRIBUTION

Huy Nguyen and Qian Wu contributed equally to this work.

This research was supported by Steelcase Inc.

DATA AVAILABILITY

The data that support the findings of this study are available from the corresponding author upon reasonable request.

REFERENCES

[1]S. E. Makris, C. L. Dym, and J. M. Smith, "Transmission loss optimization in acoustic sandwich panels," J. Acoust. Soc. Am. **79**, 1833–1843 (1986).
[2]J. Antonio, A. Tadeu, and L. Godinho, "Analytical evaluation of the acoustic insulation provided by double infinite walls," J. Sound Vib. **263**, 113–129 (2003).
[3]J. Bolton, N.-M. Shiau, and Y. Kang, "Sound transmission through multi-panel structures lined with elastic porous materials," J. Sound Vib. **191**, 317–347 (1996).
[4]L. E. Kinsler, A. R. Frey, A. B. Coppens, and J. V. Sanders, *Fundamentals of Acoustics* (Wiley, New York, 1999).
[5]M. Bruneau, *Fundamentals of Acoustics* (John Wiley & Sons, 2013).
[6]T. J. Cox and P. D'antonio, *Acoustic Absorbers and Diffusers: Theory, Design and Application* (CRC Press, 2009).
[7]L. L. Doelle, *Environmental Acoustics* (McGraw-Hill, New York, 1972).
[8]C. M. Harris, *Handbook of Acoustical Measurements and Noise Control* (McGraw-Hill, New York, 1991).
[9]S. Yao, X. Zhou, and G. Hu, "Investigation of the negative-mass behaviors occurring below a cut-off frequency," New J. Phys. **12**, 103025 (2010).
[10]S. A. Cummer, J. Christensen, and A. Alù, "Controlling sound with acoustic metamaterials," Nat. Rev. Mater. **1**, 1–13 (2016).
[11]H. Ge, M. Yang, C. Ma, M.-H. Lu, Y.-F. Chen, N. Fang, and P. Sheng, "Breaking the barriers: Advances in acoustic functional materials," Natl. Sci. Rev. **5**, 159–182 (2018).
[12]Z. Yang, J. Mei, M. Yang, N. Chan, and P. Sheng, "Membrane-type acoustic metamaterial with negative dynamic mass," Phys. Rev. Lett. **101**, 204301 (2008).
[13]Y. Chen, R. Zhu, H. Nguyen, and G. Huang, "Membrane-type acoustic metamaterials: Theory, design, and application," in *Theory and Design of Acoustic Metamaterials*, edited by P. F. Pai and G. Huang (Society of Photo Optical, Oxford, 2015), Chap. 3, pp. 53–103.
[14]N. Fang, D. Xi, J. Xu, M. Ambati, W. Srituravanich, C. Sun, and X. Zhang, "Ultrasonic metamaterials with negative modulus," Nat. Mater. **5**, 452–456 (2006).
[15]M. Yang, G. Ma, Z. Yang, and P. Sheng, "Coupled membranes with doubly negative mass density and bulk modulus," Phys. Rev. Lett. **110**, 134301 (2013).
[16]Y. Chen, G. Huang, X. Zhou, G. Hu, and C.-T. Sun, "Analytical coupled vibroacoustic modeling of membrane-type acoustic metamaterials: Membrane model," J. Acoust. Soc. Am. **136**, 969–979 (2014).
[17]H. Nguyen, R. Zhu, J. Chen, S. Tracy, and G. Huang, "Analytical coupled modeling of a magneto-based acoustic metamaterial harvester," Smart Mater. Struct. **27**, 055010 (2018).
[18]H. Nguyen, "Acoustic metasurface harvester," in *INTER-NOISE and NOISE-CON Congress and Conference Proceedings* (Institute of Noise Control Engineering, 2018), pp. 5787–5795.
[19]S. Varanasi, J. S. Bolton, T. H. Siegmund, and R. J. Cipra, "The low frequency performance of metamaterial barriers based on cellular structures," Appl. Acoust. **74**, 485–495 (2013).
[20]C. J. Naify, C.-M. Chang, G. McKnight, and S. R. Nutt, "Scaling of membrane-type locally resonant acoustic metamaterial arrays," J. Acoust. Soc. Am. **132**, 2784–2792 (2012).
[21]S. Varanasi, J. S. Bolton, and T. Siegmund, "Experiments on the low frequency barrier characteristics of cellular metamaterial panels in a diffuse sound field," J. Acoust. Soc. Am. **141**, 602–610 (2017).
[22]X. Wang, Y. Chen, G. Zhou, T. Chen, and F. Ma, "Synergetic coupling large-scale plate-type acoustic metamaterial panel for broadband sound insulation," J. Sound Vib. **459**, 114867 (2019).
[23]L. Y. L. Ang, Y. K. Koh, and H. P. Lee, "Plate-type acoustic metamaterials: Evaluation of a large-scale design adopting modularity for customizable acoustical performance," Appl. Acoust. **149**, 156–170 (2019).
[24]A. W. Leissa and M. S. Qatu, *Vibrations of Continuous Systems* (McGraw-Hill, 2011).
[25]H. Nguyen, Q. Wu, X. Xu, H. Chen, S. Tracy, and G. Huang, "Broadband acoustic silencer with ventilation based on slit-type Helmholtz resonators," Appl. Phys. Lett. **117**, 134103 (2020).
[26]G. Ma, M. Yang, S. Xiao, Z. Yang, and P. Sheng, "Acoustic metasurface with hybrid resonances," Nat. Mater. **13**, 873–878 (2014).
[27]H. Nguyen and G. Huang, "Perfect absorption in duct by coupling Helmholtz resonators," in *INTER-NOISE and NOISE-CON Congress and Conference Proceedings* (Institute of Noise Control Engineering, 2020).
[28]L. Aw, *1969 Vibration of Plates (NASA SP-160)* (U.S. Government Printing Office, Washington, DC, 1993).
[29]M. Thota and K. Wang, "Reconfigurable origami sonic barriers with tunable bandgaps for traffic noise mitigation," J. Appl. Phys. **122**, 154901 (2017).
[30]Z. Yang, H. Dai, N. Chan, G. Ma, and P. Sheng, "Acoustic metamaterial panels for sound attenuation in the 50–1000 Hz regime," Appl. Phys. Lett. **96**, 041906 (2010).